

Review

Thin Films of Homochiral Metal–Organic Frameworks for Chiroptical Spectroscopy and Enantiomer Separation

Chun Li  and Lars Heinke *

Karlsruhe Institute of Technology (KIT), Institute of Functional Interfaces (IFG),
Hermann-von-Helmholtz-Platz 1, 76344 Eggenstein-Leopoldshafen, Germany; li.chun@partner.kit.edu

* Correspondence: Lars.Heinke@kit.edu

Received: 3 April 2020; Accepted: 18 April 2020; Published: 26 April 2020



Abstract: Chiral nanoporous solids are a fascinating class of materials, allowing efficient enantiomer separation. Here, we review the status, applications, and potential of thin films of homochiral metal–organic frameworks (MOFs). Combining the advantages of MOFs, whose well-defined, crystalline structures can be rationally tuned, with the benefits of thin films enables new opportunities for the characterization of the enantioselectivity, e.g., via chiroptical spectroscopy and straightforward molecular uptake quantifications. By incorporating photoresponsive molecules in the chiral MOF films, the enantioselectivity of the material can be dynamically remote-controlled. The most promising application of MOF films is their use as membranes, where the enantioselective separation of chiral molecules is demonstrated and parameters for further improvements are discussed.

Keywords: chirality; nanoporous metal–organic frameworks; thin films and membranes; circular dichroism; enantiomer separation

1. Introduction

Enantiomer separation of chiral molecules is based on their selective interaction with a chiral medium, like a chiral surface. In addition to fundamental questions and the scientific aim of a detailed understanding, the research on enantioselective separation is driven by many important applications in pharmaceutical, agricultural, and chemical engineering [1]. Based on their large specific surface area and their tunable structure, homochiral metal–organic frameworks (MOFs) are very promising candidates for an efficient enantiomer separation. MOFs are nanoporous crystalline materials composed of metal nodes connected by organic linker molecules [2,3]. Since the first synthesis of homochiral MOFs in 1999 [4], the field of chiral MOFs has rapidly developed [5–7]. Usually homochiral MOFs are composed of chiral ligand molecules [8], but syntheses from achiral molecules or racemic mixtures are also possible [9]. Furthermore, post-synthetic modification [10] enables the modification of achiral MOFs after their synthesis to yield chiral frameworks [11,12]. In many review articles, the features and advantages of chiral MOFs have been discussed, mainly with the focus on the material in the form of powders [6,8,13–17]. The applications of chiral-MOF-powders include asymmetric catalysis, enantiomer separation using chromatography, and enantioselective adsorption of (bio-)functional molecules, like pharmaceuticals. For many applications and detailed physicochemical investigations, using the chiral MOF material in the form of thin film is beneficial, which is the topic of the present review article. In comparison to its powder equivalent, the main advantages of thin chiral MOF films are the possibilities of:

- Detailed optical investigations by UV-vis and circular dichroism (CD) spectroscopy in transmission
- Precise quantification of the enantiopure uptake by a quartz crystal microbalance (QCM)

- Enantiomer separation by pinhole-free thin membranes
- Photoresponsive chiral MOF films (which are thin enough to allow the entire irradiation by light with short penetration length)

Chiral MOF films can be prepared by various methods; for instance, by one-pot solvothermal film syntheses on the substrate, as shown in Figure 1a [18]. A particularly interesting method for the MOF film preparation is the layer-by-layer (lbl) synthesis based on liquid-phase (quasi)-epitaxy, resulting in surface-mounted MOFs (SURMOFs), as shown in Figure 1b [19,20]. There, the MOF components are consecutively deposited on an appropriately functionalized substrate. In addition to the control of the film thickness and the small surface roughness [21,22], SURMOFs typically have a low defect density, resulting in a high transparency of the material [23,24] and fast uptake and release kinetics [21,25].

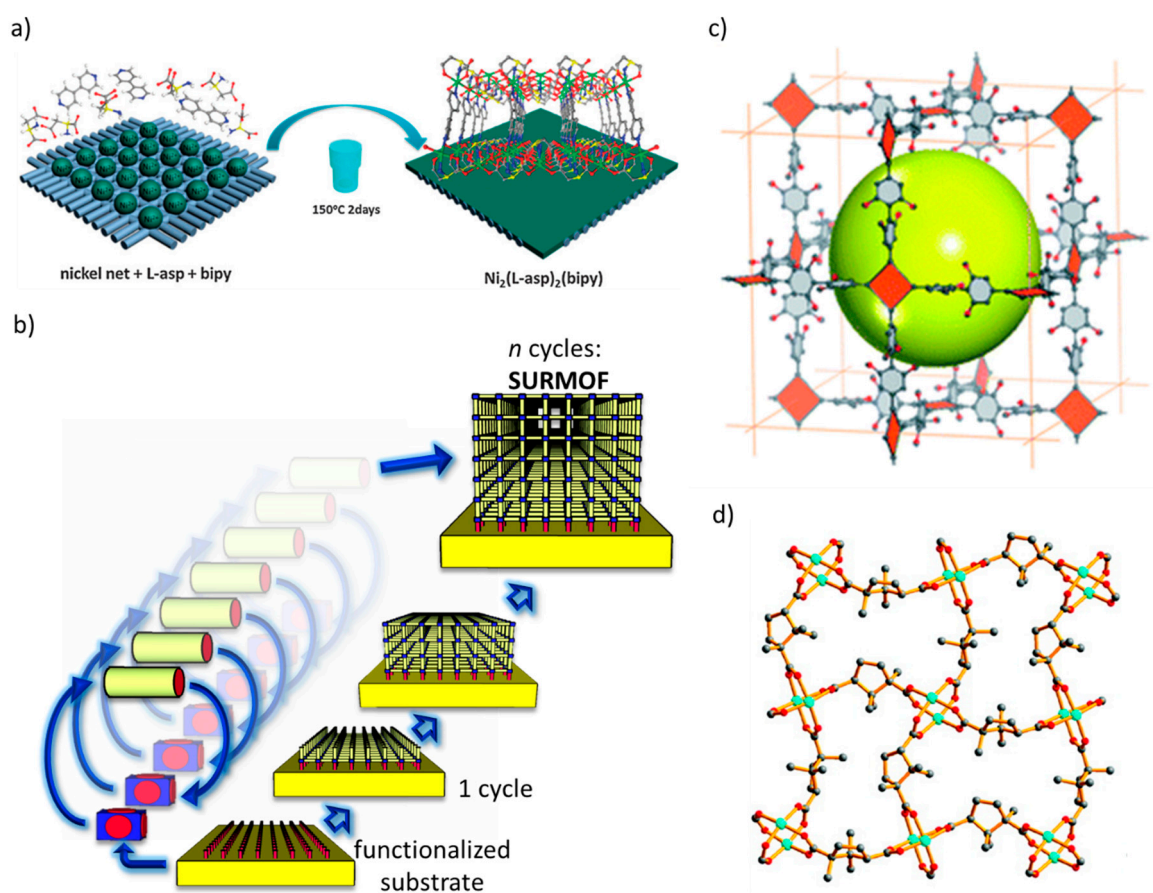


Figure 1. Syntheses of metal–organic framework (MOF) films with chiral linker molecules. (a) MOF film prepared by one-pot synthesis, where the functionalized substrate is immersed in one reaction solution. (b) Alternative sample immersion in the metal-node and in the linker solutions for many cycles results in a layer-by-layer growth of the MOF thin film, referred to as surface-mounted MOF (SURMOF). Sketches of chiral MOF structures are shown in (c) and (d). (c) (S)-KUMOF-1 ($(Cu_2(S)-1)_2(H_2O)_2$) with chiral (S)-1 ((S)-2,2'-dihydroxy-6,6'-dimethyl(1,1'-biphenyl)-4,4'-dicarboxylate) linker. (d) $Cu_2(Dcam)$ layer of $Cu_2(DCam)_2(dabco)$ (Dcam = (1*R*,3*S*)-(+)-camphoric acid; dabco = diazabicyclo[2.2.2]octane). (a) and (c) Reprinted with permissions from [18,26], Copyrights 2013 and 2011, The Royal Society of Chemistry. (b) Reprinted with permission from [20]. (d) Reprinted with permissions from [27], Copyright 2007, American Chemical Society.

2. Optical Investigation by CD Spectroscopy

Due to its small thickness, typically far below $1\mu m$, thin MOF films are transparent to some extent. In addition, the small defect density of SURMOFs increases its transparency [23,24]. As a result,

the optical properties of thin MOF films and SURMOFs can be directly measured by UV-vis spectroscopy in transmission mode. This avoids more complex methods like integrating spheres which are typically used to record UV-vis spectra of powder MOF materials. Equally simple, circular dichroism (CD) spectroscopy [28] in the UV-vis range can be applied to MOF thin films in transmission mode. Recording the MOF CD spectra in transmission mode allows the direct comparison with the spectra of the molecular components, which are typically recorded from the respective solution in the same way.

The CD spectra of PcTPDC dissolved in ethanol and incorporated in the SURMOF structure are shown in Figure 2 [29]. PcTPDC contains a planar, chiral paracyclophane moiety. Both spectra are very similar with the same characteristics. This indicates that the molecules are incorporated in the MOF structure without significant structural changes in comparison to the solvated form, keeping its chirality. A detailed inspection shows a small red-shift of the bands in the SURMOF spectrum, indicating small differences in the close proximity of the chiral moiety due to manifold reasons [30].

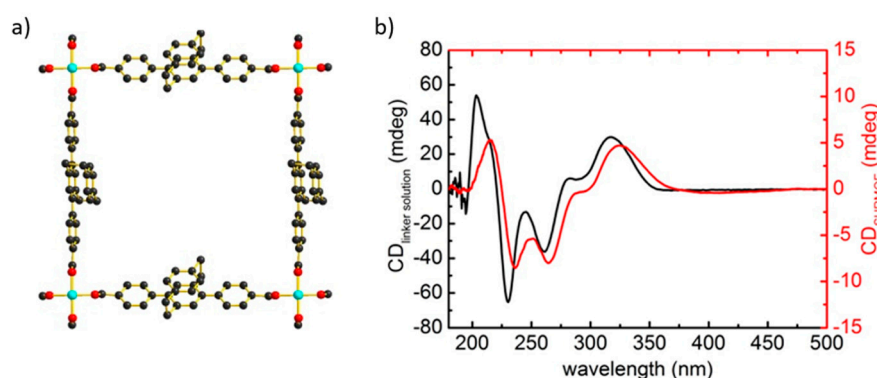


Figure 2. Planar chiral paracyclophane. (a) The structure of SURMOF-2 Cu(PcTPDC). Carbon is shown in black, oxygen in red, and copper in cyan. Hydrogen is not shown. The center ring of the terphenyl dicarboxylic acid (TPDC) linker possesses an oriented paracyclophane group, causing its chiral character. (b) The CD spectra of the PcTPDC molecule in ethanol solution (black) and in the SURMOF structure (red). Reprinted with permission from [29]. Copyright 2015, The Royal Society of Chemistry.

The SURMOF approach allows control over the crystalline growth direction by appropriate substrate functionalization, offering the opportunity to investigate the oriented CD spectra of chiral molecules along different directions. Figure 3 shows the CD spectra of $\text{Cu}_2(\text{Dcam})_2(\text{dabco})$ SURMOF measured along the crystalline [001] and [110] directions of the framework (that means perpendicular and parallel to the plane of the chiral Dcam linker molecules) [31]. The spectra for the different orientations show different intensities of the CD band. These experimental findings were also found in detailed computations of the optical excitations.

Moreover, recording the CD spectra of the chiral MOF film loaded with chiral guest molecules allows a straightforward estimation of the enantiomeric excess (*ee*) of the uptake. The spectra of $\text{Cu}_2(\text{Dcam})_2(\text{dabco})$ SURMOF loaded with ethyl-lactate in its enantiopure form, and also in its racemic mixture, are shown in Figure 3c. Comparing the empty and the loaded SURMOF CD spectra shows that the average area obtained for a 100% loading with enantiopure ethyl lactate is ± 158.5 mdeg nm, while the loading from the racemic mixture results in an area of -45 mdeg nm. As a result, an *ee*-value of 28% is estimated, implying a loading of 64% of the (+)- and 36% of the (−)-isomer.

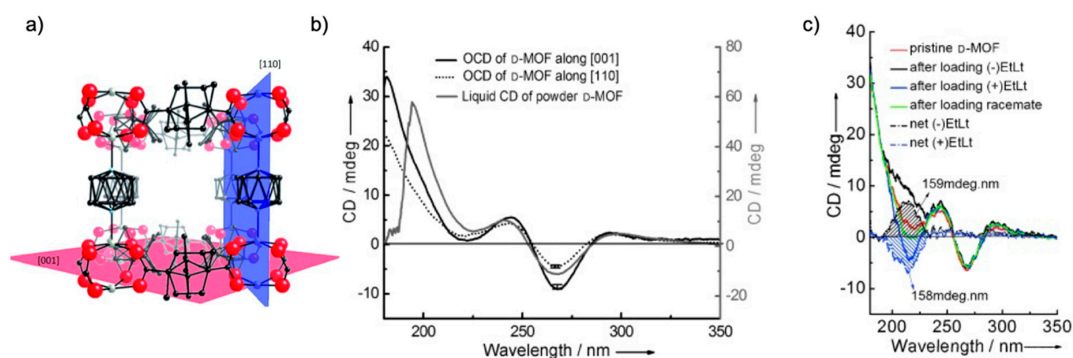


Figure 3. Oriented CD spectroscopy. (a) The structure of $\text{Cu}_2(\text{Dcam})_2(\text{dabco})$ SURMOF, where carbon is shown in black, oxygen in red, copper in grey, and nitrogen in cyan. Hydrogen is not shown. Dcam stands for D-camphoric acid, and dabco stands for 1,4-diazabicyclo[2.2.2]octane. The (001) and (110) MOF planes are indicated. (b) Oriented CD (OCD) spectra in the [001] and [110] direction. The OCD spectra are compared with the CD spectra of Dcam in ethanolic solution. (c) CD spectra of $\text{Cu}_2(\text{Dcam})_2(\text{dabco})$ SURMOF (D-MOF) in the [001] direction before (red) and after (black and blue) loading with the enantiomers and with a racemic mixture (green) of ethyl-lactate (EtLt). The dotted curves represent the difference between the CD spectrum of the pristine SURMOF and the SURMOF loaded with (+)EtLt (blue) or (−)EtLt (black). The shaded areas represent the relative net amount of the loaded enantiomers. Reprinted with permission from [31]. Copyright 2014, Wiley-VCH.

3. Precise Uptake Measurements Using a Quartz Crystal Microbalance (QCM)

The rational design and modification of MOFs allows the tuning of their pore sizes and functionalization. Due to the large porosity and specific surface area, guest molecules in the pores have strong interactions with the host MOF. For reaching efficient separation of chiral molecules, it is a highly promising path to explore and tune homochiral MOFs with the aim of high enantioselective interactions. As a measure for the enantioselectivity, the individual enantiopure uptake of both isomers by the chiral MOF material can be compared.

The uptake of guest molecules by MOF materials in the powder form can be recorded by gravimetric and volumetric techniques [32,33]. In addition, the uptake by large individual MOF crystals can be recorded by optical methods [34,35]. The molecular uptake by thin MOF films can be monitored by various techniques, like surface-plasmon resonance methods [36], X-ray diffraction [37], or spectroscopy with infrared [38] or visible [39] light.

A particularly powerful and straightforward technique is based on a quartz crystal microbalance (QCM) [40]. QCMs are typically very sensitive and can record changes of the mass density in the ng/cm^2 range. By using the SURMOF approach, the film can be grown directly on the QCM sensor, allowing the direct real-time quantification of the mass during the synthesis. By connecting the QCM to a liquid- or gas-flow system, the molecular uptake by the SURMOF from the liquid or gas phase can be measured [41,42]. Taking advantage of the mass quantification by QCM, the uptake in units of guest molecules per MOF pore (or per unit cell) can be directly calculated. Please note that the enantiopure uptake data do not allow the direct determination of the enantiomeric excess (*ee*) for the adsorption of a racemic mixture at a certain concentration, but the calculation of the *ee* value at very low loadings, in the limit of negligible small guest–guest interaction, is possible.

By using a QCM, the enantiopure uptake of (2*R*,5*R*)-2,5-hexanediol (R-HDO) and (2*S*,5*S*)-2,5-hexanediol (S-HDO) in homochiral SURMOFs of type $\text{Zn}_2(\text{Dcam})_2(\text{dabco})$ and $\text{Zn}_2(\text{Lcam})_2(\text{dabco})$, which have similar structures to their copper equivalents (see Figures 3a and 1d), was studied. The time-dependent uptake curves of R-HDO or S-HDO in the SURMOF are shown in Figure 4 [43]. While the uptake of R-HDO is approximately 1.5 times as big as the S-HDO uptake by the Dcam-SURMOF, it is opposite in the Lcam-SURMOF. The study shows that, as expected, the enantioselectivity inverts for the mirror images of the host SURMOF.

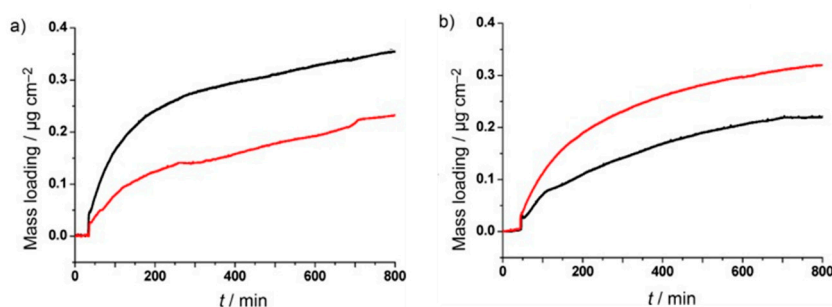


Figure 4. Enantiopure uptake of R-HDO (black) and S-HDO (red) by $\text{Zn}_2(\text{Dcam})_2(\text{dabco})$ (a) and by $\text{Zn}_2(\text{Lcam})_2(\text{dabco})$ (b). The data are recorded with a QCM. Reprinted with permission from [43]. Copyright 2012, Wiley-VCH.

In addition to the chiral center, the pore structure and the achiral components of the MOF are also crucial for the enantioselective host–guest interaction. A series of isoreticular chiral SURMOFs with identical chiral linkers but different pore sizes were prepared, namely $\text{Cu}_2(\text{Dcam})_2(\text{dabco})$, $\text{Cu}_2(\text{Dcam})_2(\text{BiPy})$, and $\text{Cu}_2(\text{Dcam})_2(\text{BiPyB})$, as shown in Figure 5 [44]. (BiPy stands for 4,4'-bipyridine and BiPyB for 1,4-bis(4-pyridyl)benzene.) While the lattice distance in the [001] direction varies between 0.95 nm and 1.8 nm, the parameters for the lattice planes perpendicular to [001] are identical. As expected, the QCM data show that the adsorption capacity of the SURMOFs increases with increasing pore size. However, the enantioselectivity does not follow such a simple trend, and the medium pore size shows the highest enantioselectivity (Figure 5d). The different enantioselectivity is caused by the different alignments of the chiral guest molecules adsorbed in the pores, where the stereogenic center has a different impact on the enantiomer selectivity. It may be hypothesized that the ideal pore size, where the chiral center has the highest impact on the host–guest interaction, resulting in the highest enantiomer separation, is roughly as large as the guest molecule. For “too” small pores, the guest molecules are “forced” to adsorb in the pores in such a position where the impact of the chiral moiety of the framework is small. For “too” large pores, the molecules can adsorb all over the large pore, and the impact of the chiral moiety is small, too (Figure 5e). A significant influence of the pore size on the enantioselectivity was also found for other MOF structures in the form of powders [45].

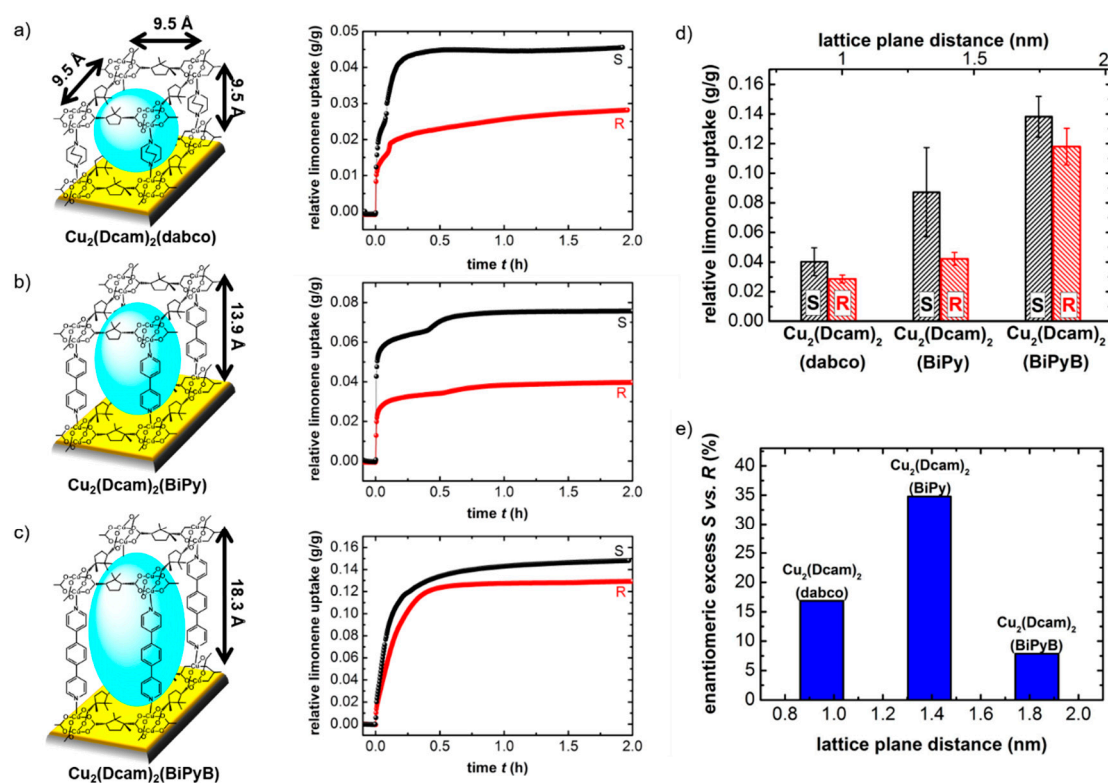


Figure 5. The effect of the pore size on the enantioselectivity. The SURMOF structure of $\text{Cu}_2(\text{Dcam})_2(\text{dabco})$ (a) $\text{Cu}_2(\text{Dcam})_2(\text{BiPy})$ (b) $\text{Cu}_2(\text{Dcam})_2(\text{BiPyB})$ (c) with the enantiopure uptake of *R*-limonene (red) and *S*-limonene (black) measured by QCM. (d) The relative uptake of limonene. The average values and the error bars representing the standard deviation of several uptake experiments are shown. (e) The enantiomeric excess for the different SURMOFs, calculated for negligible guest–guest interaction, i.e., at very small loadings. Reprinted with permission from [44]. Copyright 2015, The Royal Society of Chemistry.

4. Membrane Technology

In comparison to conventional chiral separation technologies, like enantioselective crystallization and chromatography [46–48], membrane separation technologies have the advantages of low energy consumption, large capacity, and continuous operation. Due to the tunable sharp pore size and its mechanical properties, MOFs are highly interesting materials for the membrane separation [49–51].

A chiral MOF membrane of type $\text{Zn}_2(\text{bdc})(\text{L-lac})(\text{dmf})$ was prepared on mesoporous support, where bdc denotes terephthalic acid, L-lac is L-lactate, and dmf is dimethylformamid. The separation of *R*- and *S*-methyl phenyl sulfoxide (*R*- and *S*-MPS) from *n*-hexane solution was studied, and an enantioselective enrichment of *R*-MPS in the permeate was found, as shown in Figure 6. For an *R*- and *S*-MPS feed concentration of 5 mmol L^{-1} , an enantioselective excess (*ee*) of up to 33% was obtained, showing that decent enantiomer selectivities can be achieved. Due to the diffusion-driven membrane permeation, the separation process took several hours. Increasing the concentration in the feed solution accelerated the separation process; however, the *ee* value in the permeate dropped drastically [52].

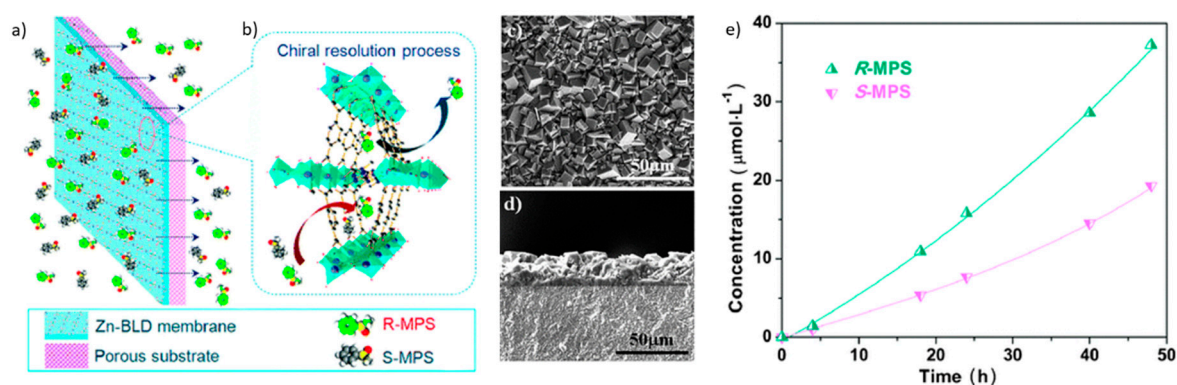


Figure 6. Enantioselective separation by homochiral MOF membranes. (a) Sketch of the supported MOF membrane with the $\text{Zn}_2(\text{bdc})(\text{l-lac})(\text{dmf})$ (Zn-BLD) MOF structure (b). Scanning electron microscopy images of the top view (c) and cross-section (d) of the membrane. (e) Permeate concentration of *R*- and *S*-methyl phenyl sulfoxide (*R*- and *S*-MPS) as a function of time. The feed concentration is 5 mmol L^{-1} . Reprinted with permission from [52]. Copyright 2012, The Royal Society of Chemistry.

Using a homochiral MOF membrane of type $\text{Ni}_2(\text{L-asp})_2(\text{BiPy})$, where L-asp denotes L-aspartic acid, racemic solutions of diols were separated using pervaporation [18]. It was found that the enantiomer selectivity is enhanced by increasing the temperature. The authors attribute this finding to the characteristics of the adsorption–diffusion model and the desorption kinetics of the isomers. By increasing the transmembrane pressure drop from 0.1 to 0.2 MPa, the *ee* value slightly decreases.

Following these pioneering studies, the enantioselective separation of different chiral molecules in the liquid phase was studied for different chiral MOF materials; a few examples are listed in Table 1. So far, the highest realized *ee* value for the permeate was obtained with a $\text{Ni}_2(\text{L-asp})_2(\text{BiPy})$ membrane. It should be noted that most practical membrane separation studies are in the liquid phase, since most pharmaceutical and biological relevant chiral molecules have a very small vapor pressure, hindering their pervaporation or gas phase membrane separation.

For industrial applications, MOF-based membranes still suffer from the slow separation and low *ee* values. Thus, it is necessary to further increase the membrane flux and selectivity. For MOF membranes, this can be done by optimizing many parameters. For example, decreasing the membrane thickness (e.g., from $25 \mu\text{m}$ [52] to less than $1 \mu\text{m}$ [58]), and increasing the active membrane area will significantly increase the throughput. Optimizing the MOF structure will also increase the flux, as well as the selectivity. Using polymer substrates [59] (and even better polymeric mixed-matrix-membranes with chiral MOF fillers [60,61]) further increases its practicality. In addition, we expected that, similar to the chiral separation in chromatography [62], the choice of the solvent is crucial for the separation process of chiral molecules in solution.

Table 1. Overview of chiral MOF films and membranes. ¹ lbl = layer-by-layer synthesis resulting in SURMOFs. ² RS = reactive seeding method. ³ The values are calculated by $ee = (S - R)/(S + R) \times 100\%$, or vice versa. ⁴ The ee value presented in the article was calculated with a different formula.

MOF Structure	Synthesis	Application and Comments	ee (%) ³	Ref.
Zn ₂ (D/Lcam) ₂ (dabco)	lbl ¹	2,5-hexanediol adsorption in film	~20	[43]
Zn(PcTPDC)	lbl ¹	limonene adsorption in film	26	[29]
Cu ₂ (D/Lcam) ₂ (dabco)	lbl ¹	oriented CD and ethyl-lactate adsorption in film	28	[31]
Cu ₂ (Dcam) ₂ (dabco)	lbl ¹	limonene adsorption in films with different pore size	8–35	[44]
Cu ₂ (Dcam) ₂ (BiPy)				
Cu ₂ (Dcam) ₂ (BiPyB)				
Cu ₂ (Dcam) ₂ (dabco)	lbl ¹	methyl lactate adsorption in film	33 ⁴	[53]
Cu ₂ (Dcam) ₂ (BiPy)				
Cu ₂ (Dcam) ₂ (AzoBiPyB)	lbl ¹	photoswitching phenylethanol adsorption in film	7–49	[54]
Zn ₂ (BDC)(L-lac)(dmf)	drop-coating of powder	phenylethanol, naphthyl ethylamine, phenyl ethylamine, methoxyphenyl ethylamine adsorption in film	15–38	[55]
Zn ₂ (BDC)(L-lac)(dmf)	RS ²	methyl phenyl sulfoxide separation by membrane	33	[52]
Ni ₂ (L-asp) ₂ (BiPy)	secondary growth	2-methyl-2,4-pentanediol separation by membrane	35.5	[56]
Ni ₂ (L-asp) ₂ (BiPy)	<i>in situ</i> growth	2-methyl-2,4-pentanediol separation by membrane at different conditions	11–32	[18]
Ni ₂ (Mal) ₂ (Bpy) ₂	RS ²	Membrane prepared	-	[57]

5. Interaction with Light: Dynamic Control of the Enantioselectivity

Following the study showing that achiral components of the MOF material also have a significant impact on the enantioselective adsorption (see chapter 3), the dynamic control of the enantioselectivity was demonstrated. To this end, photoresponsive azobenzene moieties were incorporated in homochiral D-camphorate SURMOF, resulting in Cu₂(Dcam)₂(AzoBiPyB), with AzoBiPyB denoting (*E*)-2-(phenyldiazanyl)-1,4-bis(4-pyridyl)benzene, as shown in Figure 7 [54]. The incorporation of azobenzene side groups allows the control of various MOF properties [63,64]; in particular, it allows control over the (polar) molecular interaction [65]. The azobenzene groups undergo isomerization from the thermodynamically stable *trans* form to the *cis* form, upon irradiation with UV light; and, vice versa, by thermal relaxation or by irradiation with blue light. The CD spectra (Figure 7b) show that the chirality of the MOF is not affected by the *trans*–*cis* photoswitching. This finding can be explained by the fact that the chiral and photoswitchable groups are spatially separate. In contrast to the unaffected chirality, QCM uptake experiments with *R*- and *S*-1-phenylethanol show a clear difference in the enantioselectivity upon photoswitching. While the *cis*-SURMOF shows only a small enantioselective adsorption behavior, corresponding to an ee value of $7 \pm 4\%$, the *trans*-SURMOF shows a significantly stronger adsorption of the *S*-isomer in comparison to the *R*-isomer. There, the enantioselective adsorption corresponds to an ee value of $49 \pm 15\%$. The switching effect is explained by the changes of the azobenzene dipole moment and its related interaction change; for more details, please see ref. [54]. In addition to the dynamic control of the enantioselective behavior, we foresee that this concept may help to study the interaction and the mechanism of chiral separation in MOFs.

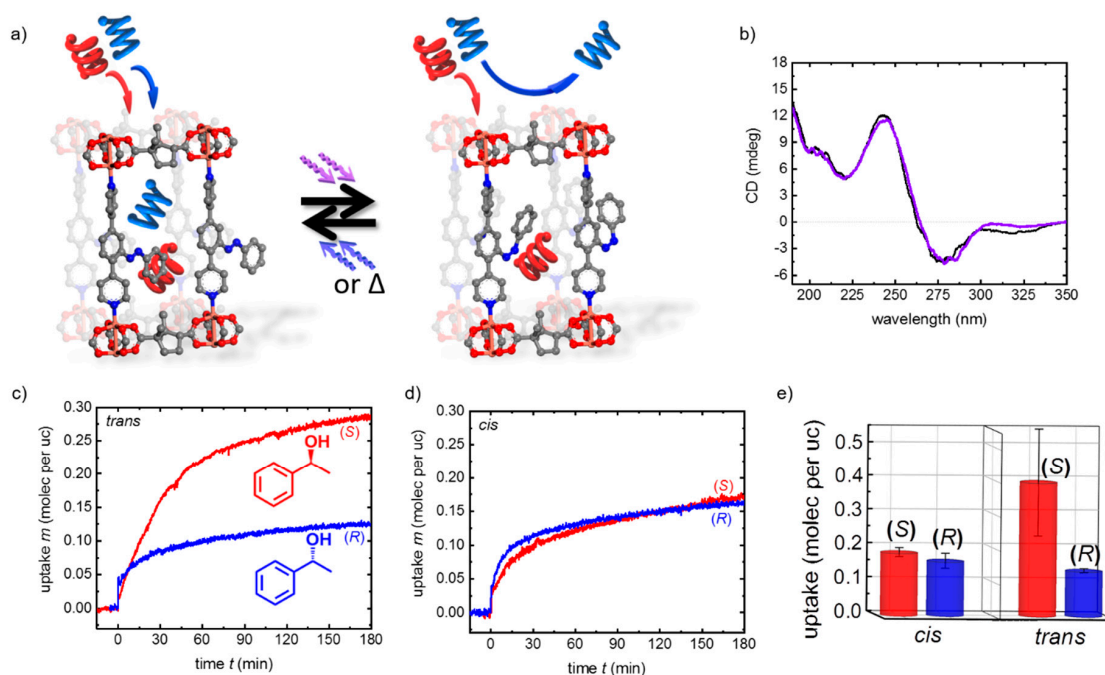


Figure 7. Photoswitching the enantioselective adsorption. (a) The $\text{Cu}_2(\text{Dcam})_2(\text{AzoBiPyB})$ SURMOF in the *trans* (left) and *cis* (right) state. (b) The CD spectra of the sample in the *trans* (black) and *cis* (violet) state. The uptake curves of the sample in the *trans* state (c) and in the *cis* state (d) for *R*- and *S*-1-phenylethanol (blue and red, respectively). (e) The average values and standard deviations of the 1-phenylethanol uptakes by the SURMOF in the *cis* and *trans* states. Reprinted with permission from [54]. Copyright 2019, The Royal Society of Chemistry.

It should be stressed that this study was enabled by several SURMOF advantages: (1) the uptake amount was quantified in a straightforward fashion by QCM; (2) the sample was sufficiently thin, allowing the characterization by CD spectroscopy; (3) the small film thickness enables irradiation of the entire sample. Since the light penetration depth in MOFs with chromophores is typically much smaller than 1 μm , only the outer shell of the MOF material would be irradiated and photoswitched in the case of MOF powders or large MOF crystals.

6. Conclusions

Chiral MOF materials demonstrate respectable enantioselective molecular interaction and are very promising for chiral separation applications. Due to their small thickness, chiral MOF thin films present a valuable model system for chiral MOFs, allowing detailed investigations which are not possible with their powder equivalent. By UV-vis absorption and chiroptical spectroscopy in transmission mode, the optical and chiral properties of the MOF material can be measured and compared with its chiral molecular components in solution. The enantioselective loading from a racemic mixture can be estimated by comparing the CD spectra of the empty and loaded MOF film. The enantiopure uptake can be quantified in a straightforward fashion using a quartz crystal microbalance. The incorporation of photoswitchable components results in the switching of the MOF properties, enabling the remote control of the enantioselectivity of the material. The potential of MOF films as membranes for an efficient separation of chiral molecules has been demonstrated, where solutions of racemic mixtures were separated with decent enantioselective enrichment in the permeate. For practical, cheap, and efficient separation processes, e.g., required for the purification of chiral pharmaceuticals, the flow-rate and the selectivity have to be further enhanced.

Currently, clear guiding principles for efficient enantiomer separation by nanoporous chiral materials are missing. Many studies (see Sections 3 and 5) show that the interaction is more complex

than the simple three-point-interaction-model. Advanced simulations and calculations have improved the understanding of the enantioselective host–guest interaction in a few cases [66–68]. Based on rapid development, significant theoretical contributions are expected within the next years. We foresee that chiral MOF films as well defined crystalline model systems, allowing precise investigations, will contribute to achieve a better understanding. In addition, we believe that chiral MOF films will contribute to advanced applications in fields like MOF-based sensors [69,70] or circularly polarized luminescence [71].

Author Contributions: Both authors contribute to this article. They have read and approved the final manuscript. All authors have read and agreed to the published version of the manuscript.

Funding: This research was funded by the German Research Foundation (DFG HE 7036/5) and the China Scholarship Council (CSC).

Conflicts of Interest: The authors declare no conflict of interest.

References

1. Stalcup, A.M. Chiral separations. *Ann. Rev. Anal. Chem.* **2010**, *3*, 341–363. [[CrossRef](#)]
2. Yaghi, O.M.; Kalmutzki, M.J.; Diercks, C.S. *Introduction to Reticular Chemistry: Metal-Organic Frameworks and Covalent Organic Frameworks*; John Wiley & Sons: Weinheim, Germany, 2019.
3. Kaskel, S. *The Chemistry of Metal-Organic Frameworks, 2 Volume Set: Synthesis, Characterization, and Applications*; John Wiley & Sons: Weinheim, Germany, 2016; Volume 1.
4. Ezuhara, T.; Endo, K.; Aoyama, Y. Helical coordination polymers from achiral components in crystals. Homochiral crystallization, homochiral helix winding in the solid state, and chirality control by seeding. *J. Am. Chem. Soc.* **1999**, *121*, 3279–3283. [[CrossRef](#)]
5. Liu, Y.; Xuan, W.M.; Cui, Y. Engineering homochiral metal-organic frameworks for heterogeneous asymmetric catalysis and enantioselective separation. *Adv. Mater.* **2010**, *22*, 4112–4135. [[CrossRef](#)] [[PubMed](#)]
6. Nickerl, G.; Henschel, A.; Grünker, R.; Gedrich, K.; Kaskel, S. Chiral metal-organic frameworks and their application in asymmetric catalysis and stereoselective separation. *Chem. Ing. Tech.* **2011**, *83*, 90–103. [[CrossRef](#)]
7. Hartlieb, K.J.; Holcroft, J.M.; Moghadam, P.Z.; Vermeulen, N.A.; Algaradah, M.M.; Nassar, M.S.; Botros, Y.Y.; Snurr, R.Q.; Stoddart, J.F. CD-MOF: A Versatile Separation Medium. *J. Am. Chem. Soc.* **2016**, *138*, 2292–2301. [[CrossRef](#)]
8. Padmanaban, M.; Müller, P.; Lieder, C.; Gedrich, K.; Grünker, R.; Bon, V.; Senkovska, I.; Baumgärtner, S.; Opelt, S.; Paasch, S.; et al. Application of a chiral metal-organic framework in enantioselective separation. *Chem. Commun.* **2011**, *47*, 12089–12091. [[CrossRef](#)]
9. Wu, S.T.; Wu, Y.R.; Kang, Q.Q.; Zhang, H.; Long, L.S.; Zheng, Z.; Huang, R.B.; Zheng, L.S. Chiral symmetry breaking by chemically manipulating statistical fluctuation in crystallization. *Angew. Chem. Int. Ed.* **2007**, *46*, 8475–8479. [[CrossRef](#)]
10. Wang, Z.Q.; Cohen, S.M. Postsynthetic modification of metal-organic frameworks. *Chem. Soc. Rev.* **2009**, *38*, 1315–1329. [[CrossRef](#)]
11. Banerjee, M.; Das, S.; Yoon, M.; Choi, H.J.; Hyun, M.H.; Park, S.M.; Seo, G.; Kim, K. Postsynthetic modification switches an achiral framework to catalytically active homochiral metal-organic porous materials. *J. Am. Chem. Soc.* **2009**, *131*, 7524–7525. [[CrossRef](#)]
12. Zhu, W.T.; He, C.; Wu, P.Y.; Wu, X.; Duan, C.Y. “Click” post-synthetic modification of metal-organic frameworks with chiral functional adduct for heterogeneous asymmetric catalysis. *Dalton Trans.* **2012**, *41*, 3072–3077. [[CrossRef](#)]
13. Leus, K.; Liu, Y.Y.; Van Der Voort, P. Metal-organic frameworks as selective or chiral oxidation catalysts. *Catal. Rev.* **2014**, *56*, 1–56. [[CrossRef](#)]
14. Gu, Z.G.; Zhan, C.H.; Zhang, J.; Bu, X.H. Chiral chemistry of metal-camphorate frameworks. *Chem. Soc. Rev.* **2016**, *45*, 3122–3144. [[CrossRef](#)] [[PubMed](#)]
15. Peluso, P.; Mamane, V.; Cossu, S. Homochiral metal-organic frameworks and their application in chromatography enantioseparations. *J. Chromatogr. A* **2014**, *1363*, 11–26. [[CrossRef](#)]

16. Duerinck, T.; Denayer, J.F.M. Metal-organic frameworks as stationary phases for chiral chromatographic and membrane separations. *Chem. Eng. Sci.* **2015**, *124*, 179–187. [[CrossRef](#)]
17. Ullah, S.; Yunus, U.; Bhatti, M.H.; Southon, P.D.; Iqbal, K.; Zaidi, S. Homochiral metal organic frameworks and their usage for the enantio-purification of racemic drugs. *ChemistrySelect* **2018**, *3*, 10434–10438. [[CrossRef](#)]
18. Kang, Z.X.; Xue, M.; Fan, L.L.; Ding, J.Y.; Guo, L.J.; Gao, L.X.; Qiu, S.L. “Single nickel source” in situ fabrication of a stable homochiral MOF membrane with chiral resolution properties. *Chem. Commun.* **2013**, *49*, 10569–10571. [[CrossRef](#)]
19. Shekhah, O.; Wang, H.; Kowarik, S.; Schreiber, F.; Paulus, M.; Tolan, M.; Sternemann, C.; Evers, F.; Zacher, D.; Wöll, C.; et al. Step-by-step route for the synthesis of metal-organic frameworks. *J. Am. Chem. Soc.* **2007**, *129*, 15118–15119. [[CrossRef](#)]
20. Heinke, L.; Wöll, C. Surface-mounted metal-organic frameworks: Crystalline and porous molecular assemblies for fundamental insights and advanced applications. *Adv. Mater.* **2019**, *31*, e1806324. [[CrossRef](#)]
21. Heinke, L.; Gu, Z.G.; Wöll, C. The surface barrier phenomenon at the loading of metal-organic frameworks. *Nat. Commun.* **2014**, *5*, 4562. [[CrossRef](#)]
22. Munuera, C.; Shekhah, O.; Wang, H.; Wöll, C.; Ocal, C. The controlled growth of oriented metal-organic frameworks on functionalized surfaces as followed by scanning force microscopy. *Phys. Chem. Chem. Phys.* **2008**, *10*, 7257–7261. [[CrossRef](#)]
23. Gu, Z.G.; Pfriem, A.; Hamsch, S.; Breitwieser, H.; Wohlgemuth, J.; Heinke, L.; Gliemann, H.; Wöll, C. Transparent films of metal-organic frameworks for optical applications. *Micropor. Mesopor. Mat.* **2015**, *211*, 82–87. [[CrossRef](#)]
24. Müller, K.; Fink, K.; Schöttner, L.; Koenig, M.; Heinke, L.; Wöll, C. Defects as color centers: The apparent color of metal-organic frameworks containing Cu²⁺-based paddle-wheel units. *ACS Appl. Mater. Inter.* **2017**, *9*, 37463–37467. [[CrossRef](#)] [[PubMed](#)]
25. Müller, K.; Vankova, N.; Schöttner, L.; Heine, T.; Heinke, L. Dissolving uptake-hindering surface defects in metal-organic frameworks. *Chem. Sci.* **2019**, *10*, 153–160. [[CrossRef](#)] [[PubMed](#)]
26. Jeong, K.S.; Go, Y.B.; Shin, S.M.; Lee, S.J.; Kim, J.; Yaghi, O.M.; Jeong, N. Asymmetric catalytic reactions by NbO-type chiral metal-organic frameworks. *Chem. Sci.* **2011**, *2*, 877. [[CrossRef](#)]
27. Zhang, J.; Yao, Y.G.; Bu, X.H. Comparative study of homochiral and racemic chiral metal-organic frameworks built from camphoric acid. *Chem. Mater.* **2007**, *19*, 5083–5089. [[CrossRef](#)]
28. Rodger, A.; Nordén, B. *Circular Dichroism and Linear Dichroism*; Oxford University Press: Oxford, UK, 1997; Volume 1.
29. Cakici, M.; Gu, Z.G.; Nieger, M.; Bürck, J.; Heinke, L.; Bräse, S. Planar-chiral building blocks for metal-organic frameworks. *Chem. Commun.* **2015**, *51*, 4796–4798. [[CrossRef](#)] [[PubMed](#)]
30. Castiglioni, E.; Abbate, S.; Longhi, G.; Gangemi, R. Wavelength shifts in solid-state circular dichroism spectra: A possible explanation. *Chirality* **2007**, *19*, 491–496. [[CrossRef](#)]
31. Gu, Z.G.; Bürck, J.; Bihlmeier, A.; Liu, J.X.; Shekhah, O.; Weidler, P.G.; Azucena, C.; Wang, Z.B.; Heissler, S.; Gliemann, H.; et al. Oriented circular dichroism analysis of chiral surface-anchored metal-organic frameworks grown by liquid-phase epitaxy and upon loading with chiral guest compounds. *Chem. Eur. J.* **2014**, *20*, 9879–9882. [[CrossRef](#)]
32. Peng, Y.; Srinivas, G.; Wilmer, C.E.; Eryazici, I.; Snurr, R.Q.; Hupp, J.T.; Yildirim, T.; Farha, O.K. Simultaneously high gravimetric and volumetric methane uptake characteristics of the metal-organic framework NU-111. *Chem. Commun.* **2013**, *49*, 2992–2994. [[CrossRef](#)]
33. Spanopoulos, I.; Bratsos, I.; Tampaxis, C.; Vourloumis, D.; Klontzas, E.; Froudakis, G.E.; Charalambopoulou, G.; Steriotis, T.A.; Trikalitis, P.N. Exceptional gravimetric and volumetric CO₂ uptake in a palladated NbO-type mof utilizing cooperative acidic and basic, metal-CO₂ interactions. *Chem. Commun.* **2016**, *52*, 10559–10562. [[CrossRef](#)]
34. Kärger, J.; Binder, T.; Chmelik, C.; Hibbe, F.; Krautscheid, H.; Krishna, R.; Weitkamp, J. Microimaging of transient guest profiles to monitor mass transfer in nanoporous materials. *Nat. Mater.* **2014**, *13*, 333–343. [[CrossRef](#)] [[PubMed](#)]
35. Chmelik, C.; Hibbe, F.; Tzoulaki, D.; Heinke, L.; Caro, J.; Li, J.; Kärger, J. Exploring the nature of surface barriers on MOF Zn(tbip) by applying ir microscopy in high temporal and spatial resolution. *Micropor. Mesopor. Mat.* **2010**, *129*, 340–344. [[CrossRef](#)]

36. He, L.H.; Duan, F.H.; Song, Y.P.; Guo, C.P.; Zhao, H.; Tian, J.Y.; Zhang, Z.H.; Liu, C.S.; Zhang, X.J.; Wang, P.Y.; et al. 2D zirconium-based metal-organic framework nanosheets for highly sensitive detection of mucin 1: Consistency between electrochemical and surface plasmon resonance methods. *2D Mater.* **2017**, *4*, 025098. [[CrossRef](#)]
37. Scherb, C.; Koehn, R.; Bein, T. Sorption behavior of an oriented surface-grown MOF-film studied by in situ X-ray diffraction. *J. Mater. Chem.* **2010**, *20*, 3046–3051. [[CrossRef](#)]
38. Kim, R.; Jee, S.; Ryu, U.; Lee, H.S.; Kim, S.Y.; Choi, K.M. Surface-enhanced infrared detection of benzene in air using a porous metal-organic-frameworks film. *Korean J. Chem. Eng.* **2019**, *36*, 975–980. [[CrossRef](#)]
39. Saghanejhadtehrani, M.; Schneider, E.K.; Heinke, L. Multi-component uptake of dye molecules by films of nanoporous metal-organic frameworks. *Chemphyschem* **2017**, *18*, 3548–3552. [[CrossRef](#)] [[PubMed](#)]
40. Johannsmann, D. *The Quartz Crystal Microbalance in Soft Matter Research. Fundamentals and Modeling*; Springer International Publishing: Cham, Switzerland, 2015.
41. Zhou, W.C.; Wöll, C.; Heinke, L. Liquid- and gas-phase diffusion of ferrocene in thin films of metal-organic frameworks. *Materials* **2015**, *8*, 3767–3775. [[CrossRef](#)]
42. Heinke, L. Diffusion and photoswitching in nanoporous thin films of metal-organic frameworks. *J. Phys. D App. Phys.* **2017**, *50*, 193004. [[CrossRef](#)]
43. Liu, B.; Shekhah, O.; Arslan, H.K.; Liu, J.X.; Wöll, C.; Fischer, R.A. Enantiopure metal-organic framework thin films: Oriented SURMOF growth and enantioselective adsorption. *Angew. Chem. Int. Edi.* **2012**, *51*, 807–810. [[CrossRef](#)]
44. Gu, Z.G.; Grosjean, S.; Bräse, S.; Wöll, C.; Heinke, L. Enantioselective adsorption in homochiral metal-organic frameworks: The pore size influence. *Chem. Commun.* **2015**, *51*, 8998–9001. [[CrossRef](#)]
45. Stylianou, K.C.; Gómez, L.; Imaz, I.; Verdugo-Escamilla, C.; Ribas, X.; MasPOCH, D. Engineering homochiral metal-organic frameworks by spatially separating 1D chiral metal-peptide ladders: Tuning the pore size for enantioselective adsorption. *Chem. Eur. J.* **2015**, *21*, 9964–9969. [[CrossRef](#)] [[PubMed](#)]
46. Porter, W.H. Resolution of chiral drugs. *Pure Appl. Chem.* **1991**, *63*, 1119–1122. [[CrossRef](#)]
47. Lorenz, H.; Seidel-Morgenstern, A. Processes to separate enantiomers. *Angew. Chem. Int. Edi.* **2014**, *53*, 1218–1250. [[CrossRef](#)]
48. Speybrouck, D.; Lipka, E. Preparative supercritical fluid chromatography: A powerful tool for chiral separations. *J. Chromatogr. A* **2016**, *1467*, 33–55. [[CrossRef](#)]
49. Bux, H.; Chmelik, C.; Krishna, R.; Caro, J. Ethene/ethane separation by the MOF membrane ZIF-8: Molecular correlation of permeation, adsorption, diffusion. *J. Membrane Sci.* **2011**, *369*, 284–289. [[CrossRef](#)]
50. Böhme, U.; Barth, B.; Paula, C.; Kuhnt, A.; Schwieger, W.; Mundstock, A.; Caro, J.; Hartmann, M. Ethene/ethane and propene/propane separation via the olefin and paraffin selective metal-organic framework adsorbents CPO-27 and ZIF-8. *Langmuir* **2013**, *29*, 8592–8600. [[CrossRef](#)]
51. Adatoz, E.; Avci, A.K.; Keskin, S. Opportunities and challenges of MOF-based membranes in gas separations. *Sep. Purif. Technol.* **2015**, *152*, 207–237. [[CrossRef](#)]
52. Wang, W.J.; Dong, X.L.; Nan, J.P.; Jin, W.Q.; Hu, Z.Q.; Chen, Y.F.; Jiang, J.W. A homochiral metal-organic framework membrane for enantioselective separation. *Chem. Commun.* **2012**, *48*, 7022–7024. [[CrossRef](#)]
53. Chen, S.M.; Liu, M.; Gu, Z.G.; Fu, W.Q.; Zhang, J. Chiral chemistry of homochiral porous thin film with different growth orientations. *ACS Appl. Mater. Inter.* **2016**, *8*, 27332–27338. [[CrossRef](#)]
54. Kanj, A.B.; Burck, J.; Grosjean, S.; Bräse, S.; Heinke, L. Switching the enantioselectivity of nanoporous host materials by light. *Chem. Commun.* **2019**, *55*, 8776–8779. [[CrossRef](#)]
55. Duan, H.J.; Yang, C.X.; Yan, X.P. Chiral metal-organic framework coated quartz crystal microbalance for chiral discrimination. *RSC Adv.* **2015**, *5*, 30577–30582. [[CrossRef](#)]
56. Huang, K.; Dong, X.L.; Ren, R.F.; Jin, W.Q. Fabrication of homochiral metal-organic framework membrane for enantioselective separation of racemic diols. *AIChE J.* **2013**, *59*, 4364–4372. [[CrossRef](#)]
57. Li, Q.Q.; Liu, G.P.; Huang, K.; Duan, J.G.; Jin, W.Q. Preparation and characterization of Ni₂(mal)₂(bpy) homochiral MOF membrane. *Asia Pac. J. Chem. Eng.* **2016**, *11*, 60–69. [[CrossRef](#)]
58. Hurrle, S.; Friebe, S.; Wohlgemuth, J.; Wöll, C.; Caro, J.; Heinke, L. Sprayable, large-area metal-organic framework films and membranes of varying thickness. *Chem. Eur. J.* **2017**, *23*, 2294–2298. [[CrossRef](#)] [[PubMed](#)]
59. Hisaki, I.; Nakagawa, S.; Sato, H.; Tohnai, N. Alignment of paired molecules of C₆₀ within a hexagonal platform networked through hydrogen-bonds. *Chem. Commun.* **2016**, *52*, 9781–9784. [[CrossRef](#)]

60. Lu, Y.Z.H.; Zhang, H.C.; Chan, J.Y.; Ou, R.W.; Zhu, H.J.; Forsyth, M.; Marijanovic, E.M.; Doherty, C.M.; Marriott, P.J.; Holl, M.M.B.; et al. Homochiral MOF-polymer mixed matrix membranes for efficient separation of chiral molecules. *Angew. Chem. Int. Ed.* **2019**, *58*, 16928–16935. [[CrossRef](#)]
61. Das, S.; Xu, S.X.; Ben, T.; Qiu, S.L. Chiral recognition and separation by chirality-enriched metal-organic frameworks. *Angew. Chem. Int. Ed.* **2018**, *57*, 8629–8633. [[CrossRef](#)]
62. Berthod, A. *Chiral Recognition in Separation Methods*; Springer: Berlin/Heidelberg, Germany, 2010.
63. Kanj, A.B.; Müller, K.; Heinke, L. Stimuli-responsive metal-organic frameworks with photoswitchable azobenzene side groups. *Macromol. Rapid Commun.* **2018**, *39*, 1700239. [[CrossRef](#)]
64. Haldar, R.; Heinke, L.; Wöll, C. Advanced photoresponsive materials using the metal-organic framework approach. *Adv. Mater.* **2019**, e1905227–e1905256. [[CrossRef](#)]
65. Wang, Z.B.; Grosjean, S.; Bräse, S.; Heinke, L. Photoswitchable adsorption in metal-organic frameworks based on polar guest-host interactions. *Chemphyschem* **2015**, *16*, 3779–3783. [[CrossRef](#)]
66. Bao, X.Y.; Broadbelt, L.J.; Snurr, R.Q. Computational screening of homochiral metal-organic frameworks for enantioselective adsorption. *Micropor. Mesopor. Mater.* **2012**, *157*, 118–123. [[CrossRef](#)]
67. Bao, X.Y.; Broadbelt, L.J.; Snurr, R.Q. Elucidation of consistent enantioselectivity for a homologous series of chiral compounds in homochiral metal-organic frameworks. *Phys. Chem. Chem. Phys.* **2010**, *12*, 6466–6473. [[CrossRef](#)] [[PubMed](#)]
68. Bueno-Perez, R.; Martin-Calvo, A.; Gómez-Álvarez, P.; Gutiérrez-Sevillano, J.J.; Merklings, P.J.; Vlugt, T.J.; van Erp, T.S.; Dubbeldam, D.; Calero, S. Enantioselective adsorption of ibuprofen and lysine in metal-organic frameworks. *Chem. Commun.* **2014**, *50*, 10849–10852. [[CrossRef](#)]
69. Gustafson, J.A.; Wilmer, C.E. Computational design of metal-organic framework arrays for gas sensing: Influence of array size and composition on sensor performance. *J. Phys. Chem. C* **2017**, *121*, 6033–6038. [[CrossRef](#)]
70. Okur, S.; Zhang, Z.J.; Sarheed, M.; Nick, P.; Lemmer, U.; Heinke, L. Towards a MOF e-Nose: A SURMOF sensor array for detection and discrimination of plant oil scents and their mixtures. *Sens. Actuators B* **2020**, *306*, 127502. [[CrossRef](#)]
71. Chen, S.M.; Chang, L.M.; Yang, X.K.; Luo, T.; Xu, H.; Gu, Z.G.; Zhang, J. Liquid-phase epitaxial growth of azapyrene-based chiral metal-organic framework thin films for circularly polarized luminescence. *ACS Appl. Mater. Inter.* **2019**, *11*, 31421–31426. [[CrossRef](#)] [[PubMed](#)]



© 2020 by the authors. Licensee MDPI, Basel, Switzerland. This article is an open access article distributed under the terms and conditions of the Creative Commons Attribution (CC BY) license (<http://creativecommons.org/licenses/by/4.0/>).